Synthesis and Asymmetric Alkene Hydrogenation Activity of C_2-Symmetric Enantioenriched Pyridine Dicarbene Iron Dialkyl Complexes

Peter Viereck, Stephan M. Rummelt, Natalia A. Soja, Tyler P. Pabst, and Paul J. Chirik*

Department of Chemistry, Princeton University, Princeton, New Jersey, 08544, U.S.A.

ABSTRACT: Enantioenriched N-alkyl-imidazole-substituted pyridine dicarbene iron dialkyl complexes have been synthesized and characterized by ^{1}H NMR and zero-field ^{57}Fe Mössbauer spectroscopies as well as single-crystal X-ray diffraction. In benzene-d_6, reversible coordination of N_2 was observed establishing an equilibrium between a five-coordinate, S = 1 iron dialkyl derivative and the corresponding six-coordinate, diamagnetic dinitrogen complex. A modest enantioselectivity of 45% ee was observed for the catalytic asymmetric hydrogenation of 1-isopropyl-1-phenyl ethylene at 4 atm of H_2 using 10 mol% of an enantioenriched iron dialkyl precatalyst, (ACNC)Fe(CH_2SiMe_3)$_2$ ((ACNC) = bis(alkylimidazol-2-ylidene)pyridine). Decreasing the H_2 pressure to 1 atm increased the enantiomeric excess to 70%. Incubation experiments established that the reaction of the iron dialkyl precatalysts with H_2 initiates a background reaction leading to the generation of a less selective catalyst; suppressing this pathway is crucial for obtaining high enantioselectivity. The attempted hydrogenation of methyl-2-acetamidoacrylate identified a deactivation pathway where N–H bond activation generated an iron alkyl κ^2-amidate alkyl. For productive catalytic reactions, deuterium labeling studies are consistent with a pathway for hydrogenation involving fast, reversible [2,1]-alkene insertion and a slow, enantiodetermining [1,2]-insertion. Monitoring the catalytic alkene hydrogenation reaction by NMR spectroscopy supports a homogeneous active catalyst that also undergoes C–H activation of the ACNC ligand backbone as a competing reaction.

INTRODUCTION

Transition-metal catalyzed asymmetric hydrogenation is a powerful method to generate enantioenriched products with applications in the fragrance, pharmaceutical, and fine-chemical industries.[1] State-of-the-art catalysts for the asymmetric alkene hydrogenation typically involve late, second or third-row transition metals, in combination with chiral phosphine or related ligands and are widely used due to their high activity, enantioselectivity and functional group tolerance (Scheme 1A).[2] Additionally, the availability of metal precursors such as [M(COD)Cl]$_2$ (M = Rh, Ir; COD = 1,5-cyclooctadiene) and reliable ligand substitution has enabled rapid and broad catalyst discovery ultimately translating onto commercial applications.[1a,f]

The discovery of catalysts based on Earth-abundant rather than precious metals has traditionally been motivated by potential advantages in cost and sustainability[3] but as new catalysts are discovered so are distinct types of reactivity[4,5] and unique mechanisms of action.[6] Although titanocene[7] and zirconocene[8] based complexes were among the first catalysts for the asymmetric hydrogenation of minimally functionalized olefins, of the Earth-abundant metal catalysts, cobalt catalysts have emerged as the most synthetically feasible. Applying a ligand design pioneered by Bianchini in olefin polymerization,[9] our laboratory reported that C_1-symmetric pyridine(diimine) cobalt alkyl complexes promote the asymmetric hydrogenation of minimally functionalized alkenes including sterically hindered examples activated by boron substituents.[10] Deuterium labeling studies on a series of indene derivatives identified a fast and reversible 2,1-insertion of the substrate into a Co–H bond that accounted for the unusual isotopic distribution of products and that 1,2-insertion was turnover limiting en route to alkane formation.[10b] Related cobalt catalysts have since been applied to the asymmetric hydrogenation of vinyl silanes,[11a] diaryl ethenes[11b] and sequential hydrofunctionalization-hydrogenation[11c-f] reactions.

Scheme 1. Metal-catalyzed asymmetric alkene hydrogenation.[2,16]

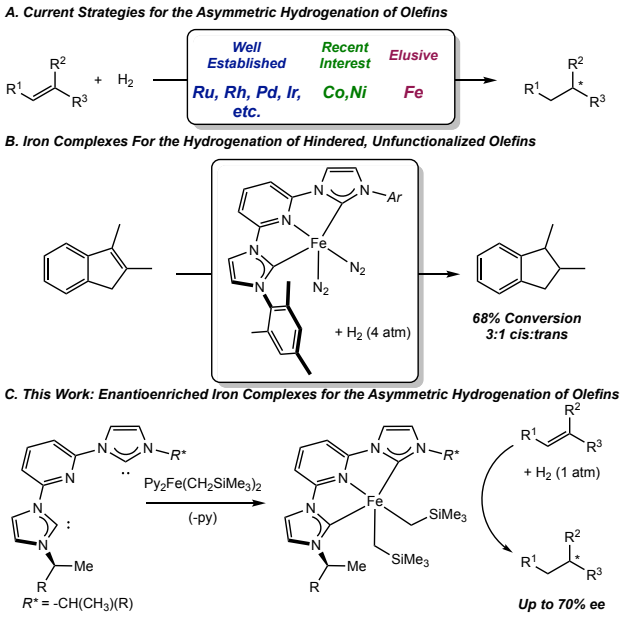

Bis(phosphine)cobalt complexes exhibit a rich asymmetric alkene hydrogenation reactivity. High-throughput experimentation (HTE) methods were applied to catalyst discovery and combinations of cobalt(II) dialkyl or combinations of cobalt(II) halides with zinc reductants generated highly active and enantioselective catalysts for the hydrogenation of host of functionalized alkenes.[5a] Notable examples include the enantioselective synthesis of Levetiracetam on 200-gram scale in methanol solution with performance superior to rhodium catalysts as well as the hydrogenation of α,β-unsaturated carboxylic acid derivatives including several drug precursors.[5e]

Attempts to translate the design principles from bis(phosphine)cobalt-catalyzed asymmetric alkene hydrogenation of olefins to iron have been met with limited success. While preparation of bis(phosphine)iron(II) dialkyl derivatives proved relatively straightforward, treatment of these compounds with dihydrogen in the presence of alkene resulted in rapid formation of heterogeneous iron catalysts that promoted essentially racemic hydrogenation reactions.[12] These results suggested that strong field tridentate pincer ligands, by virtue of their higher affinity for the metal center, may result in more long-lived and robust homogeneous hydrogenation catalysts. Indeed, several examples of iron-catalyzed asymmetric alkene hydrofunctionalizations,[13] and iron-catalyzed asymmetric C=X reduction[14] are reported. However, the iron-catalyzed asymmetric hydrogenation of alkenes with synthetically useful enantioselectivity (>80% ee) remains elusive.[2]

Aryl-substituted, C_{2v}-symmetric pyridine(diimine) iron dinitrogen complexes provided early examples of catalysts for the hydrogenation of alkenes at, in some cases at part per million loadings of iron.[15] By replacing the imine donors of the tridentate pincers with more donating N-heterocyclic carbenes (NHC), Danopoulos and coworkers introduced a more electron-rich dinitrogen complex, (^{iPr}CNC)Fe$(N_2)_2$.[16] Our laboratory later demonstrated that this class of complexes was among the most active Earth abundant metal catalysts for the hydrogenation of hindered, minimally functionalized alkenes[17a] and the active catalytic species were identified by ^{1}H NMR spectroscopy and single-crystal X-ray diffraction.[17b] Recently iron(II) dialkyl derivatives, (^{Ar}CNC)Fe$(CH_2SiMe_3)_2$ have been synthesized, obviating the need for strong alkali metal reductants and the extreme air and moisture sensitivity of dinitrogen derivatives.[17c] This synthetic approach has also proven more versatile, being compatible with more chelate variants than alkali metal reductions that form iron dinitrogen compounds.

Here we describe application of this method to the synthesis and characterization of enantioenriched, C_2-symmetric (ACNC)Fe$(CH_2SiMe_3)_2$ ((ACNC) = bis(alkylimidazol-2-ylidene)pyridine) iron complexes and explore their utility for the asymmetric hydrogenation of alkenes. Equilibria between the five-coordinate, S = 1 iron dialkyl complexes and the corresponding six-coordinate, S = 0 dinitrogen derivatives was identified in solution. The enantioselectivity of the alkene hydrogenation increased as the pressure of H_2 was decreased. Deuterium labeling studies established that C–H activation of the solvent is competitive with alkene hydrogenation.

RESULTS AND DISCUSSION

Our studies commenced with the preparation of a series of ACNC[18] ligands by a nucleophilic aromatic substitution of the corresponding imidazoles to 2,6-dibromopyridine, and subsequently deprotonation by KHMDS.[17c] Metallation of the ACNC ligands was accomplished by addition of the free dicarbene of the pincer to a pentane solution of freshly prepared py$_2$Fe$(CH_2SiMe_3)_2$ (py = pyridine; Scheme 2A).[19] The resulting iron dialkyl complexes precipitated from pentane as microcrystalline red-brown or dark purple solids. A representative achiral example, (^{iPr}ACNC)Fe$(CH_2SiMe_3)_2$ was included in this study for comparison.

Scheme 2. A. Preparation of (ACNC)Fe$(CH_2SiMe_3)_2$[a] **B.** Solid-state structure of ($^{(S)\text{-}tBu,Me}$ACNC)Fe$(CH_2SiMe_3)_2(N_2)$ at 30% probability ellipsoids. Hydrogen atoms attached to stereogenic centers omitted for clarity.

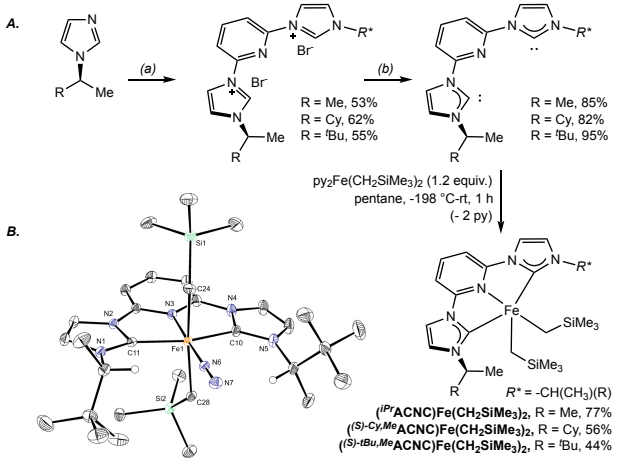

[a]Reagents and conditions: (a) 2,6-dibromopyridine, 150 °C, 48 h. (b) KHMDS, THF -110 °C to RT, 1 h.

Solution magnetic moments (Evans method) between 2.7 and 2.8 μB were measured for all three iron dialkyl complexes at 23 °C under vacuum, consistent with two unpaired electrons and S = 1 ground states. Accordingly, all three compounds exhibited paramagnetically broadened and shifted resonances in the ambient temperature benzene-d_6 NMR spectra. However, for all three iron dialkyl derivatives, a strong N≡N band was observed in the benzene solution infrared spectrum (Figure 1), consistent with coordination of dinitrogen. The signals for ($^{(S)\text{-}tBu,Me}$ACNC)Fe$(CH_2SiMe_3)_2$ under a nitrogen atmosphere were significantly broadened such that assignment of the signals was challenging. Freeze-pump-thawing the solution and recording the ^{1}H NMR spectrum under static vacuum sharpened these signals, indicating a fast and reversible coordination of N_2 in benzene solution. Cooling a toluene-d_8 solution of ($^{(S)\text{-}tBu,Me}$ACNC)Fe$(CH_2SiMe_3)_2$ to -80 °C under 1 atm of N_2 produced signals consistent with a

diamagnetic compound, assigned to formation of a 6-coordinate, $S = 0$ iron dinitrogen complex (Figure S27). This behavior contrasts (^{tBu}ACNC)Fe(CH_2SiMe_3)$_2$, a previously reported diamagnetic compound with an unusual square pyramidal geometry that provided no evidence for N_2 coordination in solution or the solid state.[17c]

Single crystals of ($^{(S)\text{-}tBu,Me}$ACNC)Fe(CH_2SiMe_3)$_2$(N_2) suitable for X-ray diffraction were obtained from a concentrated Et_2O-pentane solution stored at -30 °C. The solid-state structure (Scheme 2B) confirmed the idealized octahedral geometry with a dinitrogen ligand coordinated *trans* to the pyridine of the pincer. This geometry is consistent with previously reported (^{Ar}CNC)Fe(CH_2SiMe_3)$_2$(N_2) complexes.[17c] Unfortunately, attempts to obtain single crystals of the five-coordinate dialkyl complexes have been unsuccessful.

The neopentyl analogue of ($^{(S)\text{-}tBu,Me}$ACNC)Fe(CH_2SiMe_3)$_2$ was prepared using an analogous procedure with freshly prepared py$_2$Fe(CH_2CMe_3)$_2$.[20] A red solid identified as ($^{(S)\text{-}tBu,Me}$ACNC)Fe(CH_2CMe_3)$_2$(N_2) was isolated in 66% yield and exhibited ^{1}H and ^{13}C NMR resonances consistent with a diamagnetic compound (Scheme 3). Unlike the silicon-containing congener, no color change was observed under vacuum and the N-N band at 2068 cm^{-1} persisted in the benzene solution infrared spectrum. The subtle differences in the identity of the alkyl ligand and the impact on dinitrogen coordination is likely due to the decreased electron donating ability of the neopentyl ligands which permit dinitrogen coordination.

Scheme 3. Preparation of ($^{(S)\text{-}tBu,Me}$ACNC)Fe(CH_2CMe_3)$_2$(N_2).

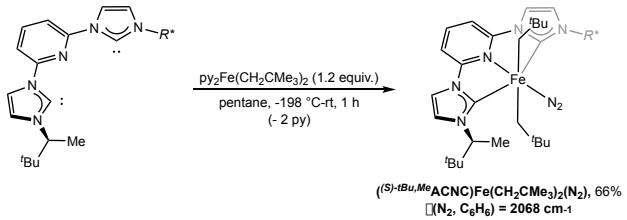

Zero-field ^{57}Fe Mössbauer spectroscopy was used to further study the electronic structures and dinitrogen coordination behavior of the iron dialkyl complexes. (Figure 1, Table 1). The solid-state spectrum of (^{iPr}ACNC)Fe(CH_2SiMe_3)$_2$ contained a major component (78 %) with an isomer shift of δ = 0.11 mm/s and a quadrupole splitting of $|\Delta E_Q|$ = 2.56 mm/s, assigned to the 5-coordinate, $S = 1$ iron dialkyl. These values were in agreement with DFT calculations on full molecular models (δ = 0.12 mm/s, ΔE_Q = -2.43 mm/s, B3LYP). The minor component, comprising 22% of the sample, exhibited an isomer shift of δ = 0.19 mm/sand a quadrupole splitting of $|\Delta E_Q|$= 1.20 mm/s (calculated δ = 0.17 mm/s, ΔE_Q = 1.65 mm/s, B3LYP), values that compare to those reported previously for low-spin (^{Ar}CNC)Fe(CH_2SiMe_3)$_2$(N_2) compounds.[17c] For ($^{(S)\text{-}Cy,Me}$ACNC)Fe(CH_2SiMe_3)$_2$, the major component (59 %) has an isomer shift of δ = 0.15 mm/s and a quadrupole splitting of $|\Delta E_Q|$ = 1.61 mm/s (calculated δ = 0.18 mm/s, ΔE_Q = 1.62 mm/s, B3LYP), consistent with the 6-coordinate, low-spin iron(II) dinitrogen complex, while the parameters (δ = 0.13 mm/s; $|\Delta E_Q|$ = 2.46 mm/s; calculated δ = 0.13 mm/s, ΔE_Q = -2.35 mm/s B3LYP) for the minor compound (41%) correspond to the $S = 1$ five-coordinate iron dialkyl. For ($^{(S)\text{-}tBu,Me}$ACNC)Fe(CH_2SiMe_3)$_2$, the major component in the solid state (76%) is the 6-coordinate, iron(II) dinitrogen complex (δ = 0.13 mm/s; $|\Delta E_Q|$ = 1.53 mm/s; calculated δ = 0.19 mm/s, ΔE_Q = 1.52 mm/s, B3LYP), while the minor component (24%) corresponds to the 5-coordinate S=1 iron dialkyl (δ = 0.14 mm/s; $|\Delta E_Q|$ = 2.43 mm/s; calculated δ = 0.15 mm/s, ΔE_Q = -2.40 mm/s, B3LYP). With the neopentyl analogue, ($^{(S)\text{-}tBu,Me}$ACNC)Fe(CH_2CMe_3)$_2$(N_2), only the 6-coordinate dinitrogen complex was observed, with an isomer shift of δ = 0.10 mm/s and a quadrupole splitting of $|\Delta E_Q|$ = 1.55 mm/s was observed consistent with exclusive formation of the diamagnetic, 6-coordinate complex.

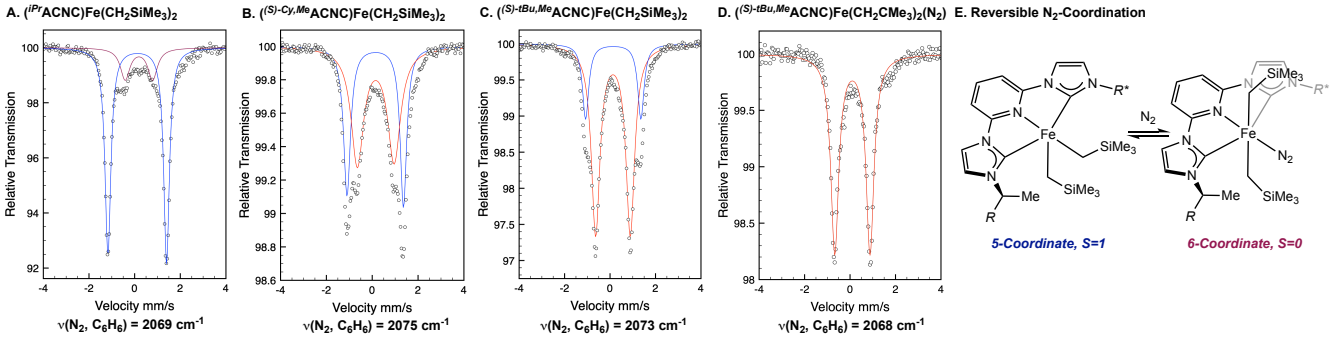

Figure 1. Solid-state zero-field ^{57}Fe Mössbauer spectra and infrared N≡N stretching frequencies of **A.** (^{iPr}ACNC)Fe(CH_2SiMe_3)$_2$ **B.** ($^{(S)\text{-}Cy,Me}$ACNC)Fe(CH_2SiMe_3)$_2$ **C.** ($^{(S)\text{-}tBu,Me}$ACNC)Fe(CH_2SiMe_3)$_2$ **D.** ($^{(S)\text{-}tBu,Me}$ACNC)Fe(CH_2CMe_3)$_2$(N_2) **E.** Reversible N_2-coordination in (ACNC)Fe(CH_2SiMe_3)$_2$.

Table 1. Solid-state zero-Field ^{57}Fe Mössbauers of alkyl-substituted pyridine dicarbene iron complexes.

[Fe]	δ (mm/s)	$\lvert\Delta E_Q\rvert$ (mm/s)
(^{iPr}ACNC)Fe(CH_2SiMe_3)$_2$ (78%)	0.11	2.56
(^{iPr}ACNC)Fe(CH_2SiMe_3)$_2$(N_2) (22%)	0.19	1.20
($^{(S)\text{-}Cy,Me}$ACNC)Fe(CH_2SiMe_3)$_2$ (59%)	0.13	2.46
($^{(S)\text{-}Cy,Me}$ACNC)Fe(CH_2SiMe_3)$_2$(N_2) (41%)	0.15	1.61
($^{(S)\text{-}tBu,Me}$ACNC)Fe(CH_2SiMe_3)$_2$ (24%)	0.14	2.43
($^{(S)\text{-}tBu,Me}$ACNC)Fe(CH_2SiMe_3)$_2$(N_2) (76%)	0.13	1.53
($^{(S)\text{-}tBu,Me}$ACNC)Fe(CH_2CMe_3)$_2$(N_2) (>95%)	0.10	1.55

The behavior of (ACNC)Fe(CH_2SiMe_3)$_2$ upon treatment with strong L-type donors was explored. Exposure of aryl-substituted (CNC)Fe(CH_2SiMe_3)$_2$(N_2) complexes to carbon monoxide does not induce reductive elimination of the alkyl ligands, but instead results in ligand substitution to yield (CNC)Fe(CH_2SiMe_3)$_2$(CO).[17c] Likewise, exposure of a benzene-d_6 solution of ($^{(S)\text{-}tBu,Me}$ACNC)Fe(CH_2SiMe_3)$_2$ to 1 atm of CO generated ($^{(S)\text{-}tBu,Me}$ACNC)Fe(CH_2SiMe_3)$_2$(CO) (Scheme 4A). A strong CO band centered at 1903 cm^{-1} was observed in the benzene solution infrared spectrum. Single crystals of ($^{(S)\text{-}tBu,Me}$ACNC)Fe(CH_2SiMe_3)$_2$(CO) were obtained from a toluene-pentane mixture stored at -35 °C and the solid-state structure confirms an analogous idealized octahedral geometry similar to (ACNC)Fe(CH_2SiMe_3)$_2$(N_2), where CO occupies the site *trans* to the pyridine donor of the ACNC pincer (Scheme 4B).

Scheme 4. A. Synthesis of ($^{(S)\text{-}tBu,Me}$ACNC)Fe(CH_2SiMe_3)$_2$(CO). **B.** Solid-Structure of ($^{(S)\text{-}tBu,Me}$ACNC)Fe(CH_2SiMe_3)$_2$(CO)**.** Thermal ellipsoids at 30 % probability. Hydrogen atoms attached to stereogenic centers omitted for clarity.

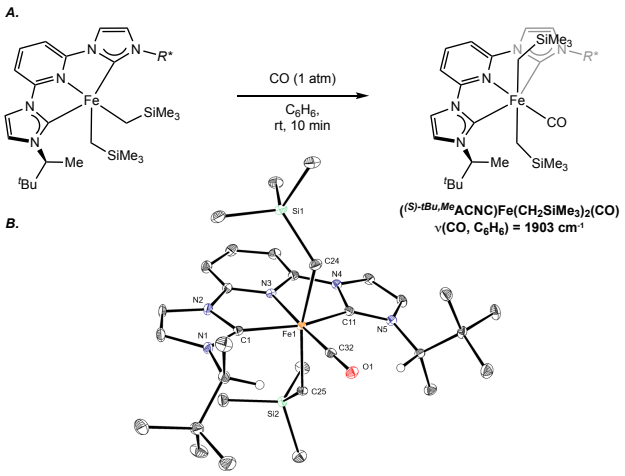

Both ($^{(S)\text{-}Cy,Me}$ACNC)Fe(CH_2SiMe_3)$_2$ and ($^{(S)\text{-}tBu,Me}$ACNC)Fe(CH_2SiMe_3)$_2$ were evaluated for catalytic asymmetric alkene hydrogenation. The 1,1-disubstituted alkene (1-isopropylvinyl)benzene (**1a**) was selected as a representative substrate due to its previous use in asymmetric hydrogenation with related cobalt catalysts.[10a] Initial conditions employed 10 mol% of the iron dialkyl precatalyst with 4 atm of H_2 in benzene-d_6 solution. With ($^{(S)\text{-}Cy,Me}$ACNC)Fe(CH_2SiMe_3)$_2$, complete conversion to the alkane was observed after 30 minutes. An enantiomeric excess of 40% was obtained favoring the (*R*)-isomer of the alkane product (Scheme 5). Similar activity was observed with ($^{(S)\text{-}tBu,Me}$ACNC)Fe(CH_2SiMe_3)$_2$ and under identical catalytic conditions, the *ee* increased to 45%. Decreasing the H_2 pressure with the latter iron precatalyst *increased* the *ee* to 70%. Curiously, the related precatalyst, ($^{(S)\text{-}tBu,Me}$ACNC)Fe(CH_2CMe_3)$_2$(N_2) gave significantly lower enantioselectivity (48% ee), suggesting that precatalyst activation may play a significant role in catalyst performance (vide infra).

Scheme 5. Evaluation of enantioenriched (ACNC)Fe complexes for asymmetric alkene hydrogenation**.**

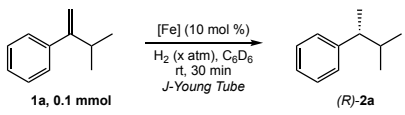

[Fe]	P (atm)	% conv.	% ee
($^{(S)\text{-}Cy,Me}$ACNC)Fe(CH_2SiMe_3)$_2$	4	>95	40
($^{(S)\text{-}tBu,Me}$ACNC)Fe(CH_2SiMe_3)$_2$	4	>95	45
($^{(S)\text{-}tBu,Me}$ACNC)Fe(CH_2SiMe_3)$_2$	1	>95	70
($^{(S)\text{-}tBu,Me}$ACNC)Fe(CH_2CMe_3)$_2$(N_2)	1	>95	48

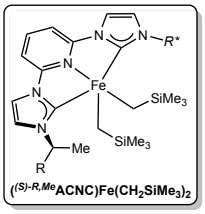

Inspired by these observations, conditions favoring lowering H_2 pressures while maintaining an excess of dihydrogen, were explored. A series of hydrogenation reactions of **1a** were conducted in thick-walled glass vessels with 0.1, 0.5, 1 and 4 atm of H_2 using ($^{(S)\text{-}tBu,Me}$ACNC)Fe(CH_2SiMe_3)$_2$ as the precatalyst. Decreasing enantiomeric excesses were observed with increasing pressure, further confirming the inverse H_2 pressure dependence on enantioselectivity (Scheme 6). The highest enantioselectivity (70% *ee*) was observed when a J. Young NMR

tube was used as the reaction vessel and mixed only by vertical rotation. These results demonstrate the impact of *the mass transfer of hydrogen* on the levels of enantioselectivity.[21] A variety of conditions were evaluated including: catalyst loading, solvent, and temperatures (See SI). In each case, however no improvement in enantioselectivity was observed.

Scheme 6. Effect of hydrogen pressure on enantioselectivity.

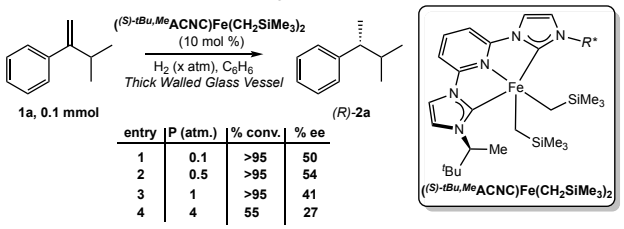

entry	P (atm.)	% conv.	% ee
1	0.1	>95	50
2	0.5	>95	54
3	1	>95	41
4	4	55	27

One plausible explanation for the observed inverse hydrogen dependence is a competing, productive olefin isomerization process which becomes more prominent at lower hydrogen pressures. To rule out this hypothesis, the hydrogenation reaction was conducted at substoichiometric quanitities of hydrogen gas. One notable observation in the hydrogenation of **1a** with $(^{(S)\text{-}tBu,Me}\text{ACNC})\text{Fe}(\text{CH}_2\text{SiMe}_3)_2$ and 0.1 atm H_2 gas is that *deuterium* incorporation was observed in the methylene position of the alkene (**1a-*d*$_2$**: 31%), as well as in the benzylic position (43%) and methyl groups (50%) of the resulting alkane (Scheme 7A). Our laboratory has previously reported that $[(^{Ar}\text{CNC})\text{Fe}]$ complexes are active for C(sp^2)–H hydrogen isotope exchange (HIE) using benzene-d_6 as the deuterium source.[4d] The C–D activation of the benzene-d_6 solvent is competitive with olefin insertion when the hydrogen pressure is lowered, resulting in deuterium incorporation of the alkene. No improvement of the enantioselectivity from the 1 atm conditions was observed (64% *ee*). Deuteration of **1a** with 1 atm of D_2 gas at 23 °C in the presence of 10 mol% of $(^{(S)\text{-}tBu,Me}\text{ACNC})\text{Fe}(\text{CH}_2\text{SiMe}_3)_2$ produced the alkane in 62% *ee* with near complete deuteration of the benzylic and methyl positions (Scheme 7B). A similar deuterium incorporation pattern was observed when the catalytic reaction was conducted at 4 atm of D_2 but the *ee* eroded to 50%. Importantly, no isomerized alkene was observed during the course of the hydrogenation reactions. Consistent with this observation, no deuterium was observed in the homobenzylic methine position of alkane, demonstrating that alkene isomerization is *not* the source of the higher *ee* observed at lower pressures of H_2. The observed positions of deuterium incorporation demonstrate that the hydrogenation reaction proceeds with fast and reversible 2,1-insertion and that 1,2-insertion is likely turnover limiting and enantiodetermining.[3d] A stereochemical model rationalizing the moderate selectivity for the *(R)*-enantiomer is presented in Figure S38. Additional experimental and computational data are needed to support this model. The origin of the inverse dependence between H_2 pressure and enantioselectivity will be discussed below.

Scheme 7. A. Effect of substoichiometric quantities of hydrogen. **B.** Deuterium labeling studies**.**

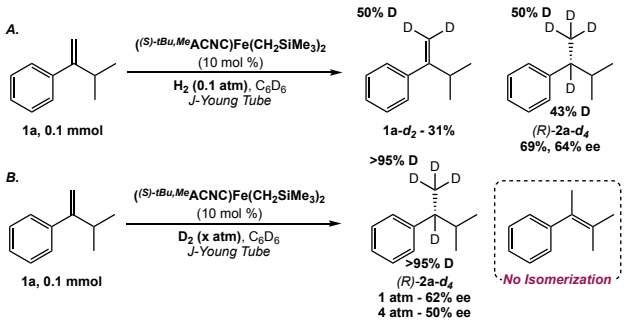

Other 1,1-disubstituted alkenes, and trisubstituted alkenes were evaluated for iron-catalyzed asymmetric alkene hydrogenation (Scheme 8). With the goal of potentially slowing reactivity and increasing the overall enantioselectivity, alkene **1b**, a more hindered analogue of **1a,** was subjected to the standard catalytic hydrogenation conditions. Slightly reduced activity (70% conversion to alkane, 17 hours) and lower *ee* (28%) were observed. The less hindered 1,1-disubstituted alkene, **1c** produced higher conversion (>95%, 30 min) but with negligible enantioselectivity (~5% *ee*). Trisubstituted alkenes **1d** and **1e** also underwent hydrogenation with poor enantioselectivity (13%, 16% *ee* respectively), despite the slower reaction.

Scheme 8. $(^{(S)\text{-}tBu,Me}\text{ACNC})\text{Fe}(\text{CH}_2\text{SiMe}_3)_2$ as a precatalyst for the asymmetric hydrogenation of 1,1-disubstituted, and trisubstituted alkenes.

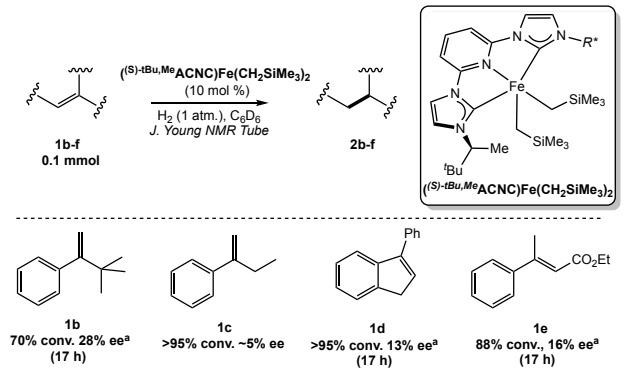

[a]Average of two runs

The hydrogenation of methyl-2-acetamidoacrylate (MAA, **1f**) was also studied to gain insight into to the functional group tolerance of the iron catalysts and due to the previous success of the activated alkenes in precious metal and cobalt-catalyzed reactions.[5a] Addition of **1f** to a benzene-d_6 solution of $(^{(S)\text{-}tBu,Me}\text{ACNC})\text{Fe}(\text{CH}_2\text{SiMe}_3)_2$ produced a distinct color change from red to purple. The newly formed purple product was independently synthesized and assigned as the iron MAA complex, $(^{(S)\text{-}tBu,Me}\text{ACNC})\text{Fe}(\text{CH}_2\text{SiMe}_3)(\text{MAA})$, based on ^{1}H and ^{13}C NMR spectroscopy and single-crystal X-ray diffraction (Scheme 9). This complex arises from the protonation of one of the neosilyl ligands of $(^{(S)\text{-}tBu,Me}\text{ACNC})\text{Fe}(\text{CH}_2\text{SiMe}_3)_2$ and coordination of the amidate. $(^{(S)\text{-}tBu,Me}\text{ACNC})\text{Fe}(\text{CH}_2\text{SiMe}_3)(\text{MAA})$ proved unreactive to H_2 and HBPin even at elevated temperatures (80 °C) and is air stable (~5 hours) in the solid state, showing discoloration to from a purple to a brown color after this time. Utilizing $(^{(S)\text{-}tBu,Me}$

ACNC)Fe(CH_2SiMe_3)(MAA) as a precatalyst for hydrogenation of **1a** resulted in a slow reaction along with poor (<5% *ee*) enantioselectivity. Thus this protonation event is identified as a deactivation pathway and any hydrogenation reactivity may be the result of an unidentified iron decomposition product.

Scheme 9. A. Synthesis of ($^{(S)\text{-}tBu,Me}$ACNC)Fe(CH_2SiMe_3)(MAA). **B.** Solid-state structure of ($^{(S)\text{-}tBu,Me}$ACNC)Fe(CH_2SiMe_3)(MAA) at 30 % probability ellipsoids. Hydrogen atoms attached to stereogenic centers omitted for clarity.

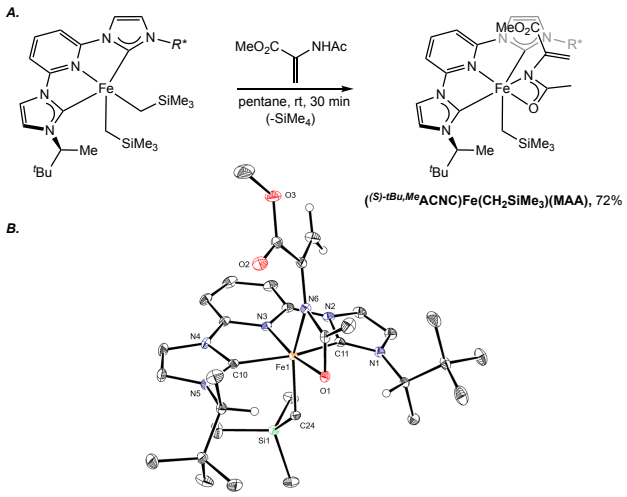

Investigations into the catalyst speciation, specifically the iron product formed following treatment of the iron dialkyl with H_2, were undertaken. Aryl-substituted [(CNC)Fe] compounds are known to form the corresponding (CNC)Fe(H)$_2$(η^2-H_2) and (CNC)Fe(H)$_2$(N_2) derivatives upon exposure to dihydrogen.[17b] Treatement of a benzene solution of $^{(S)\text{-}tBu,Me}$ACNC)Fe(CH_2SiMe_3)$_2$ with 1 atm of H_2 followed by rapidly freezing and analysis by zero-field ^{57}Fe Mössbauer spectroscopy revealed a complex mixture of products (Figure S9).

Exposure of a benzene-d_6 solution of ($^{(S)\text{-}tBu,Me}$ACNC)Fe(CH_2SiMe_3)$_2$ to 1 atm of H_2 at 23 °C immediately generated $SiMe_4$ with concomitant disappearance of *all* of the signals in the ^{1}H NMR spectrum corresponding to the iron compound. Treatment of this product with excess carbon monoxide resulted in rapid formation of a new, diamagnetic product in 82% yield identified as d_3-($^{(S)\text{-}tBu,Me}$ACNC)Fe(CO)$_2$-d_3 in 82 % NMR yield, where complete deuteration at the 2,4, and 6 position of the ligand backbone is observed (Scheme 10A). Diagnostic CO bands were observed at 1907 and 1863 cm^{-1} in the benzene solution infrared spectrum. To gain insight into the factors affecting catalyst lifetime, this combined hydrogenolysis-carbonylation reaction was performed at a variety of hydrogen treatment times and pressures, as the yield of $^{(S)\text{-}tBu,Me}$ACNC)Fe(CO)$_2$-d_3 after hydrogenolysis likely directly correlates to the amount of homogeneous iron in solution. After 10 minutes of reaction time, at 1 and 4 atmospheres of hydrogen produced 82%, and 42% NMR yield respectively (Scheme 10a, entry 1 and 2), demonstrating that increasing the concentration of hydrogen in solution decreases the quantity of active catalyst. At 1 atm of H_2 gas, at increasing reaction time, the yield of ($^{(S)\text{-}tBu,Me}$ACNC)Fe(CO)$_2$-d_3 decreased from 82%, to 54% (Scheme 10a, entry 1, 3-5), confirming that the homogeneous iron species decomposes under excess H_2 gas. Performing the hydrogenation reaction in cyclohexane-d_{12} also generated an NMR silent iron product and a complex mixture was observed by ^{1}H NMR spectroscopy after treatment with CO. Related aryl-substituted pincer iron complexes, [(^{Ar}CNC)Fe] are known to form trans-dihydride η^2-dihydrogen complexes upon treatment of the dinitrogen or dialkyl complexes with H_2.[17b] It is likely that a similar pathway is operative with the enantioenriched C_2-symmetric examples reported here, however rapid C–H activation and hydrogen isotope exchange processes with the deuterated solvents complicate the spectroscopic characterization.

With the hydrogen-induced decomposition of ($^{(S)\text{-}tBu,Me}$ACNC)Fe(CH_2SiMe_3)$_2$ established, possible background catalytic reactions arising from these newly formed iron products were evaluated. Benzene-d_6 solutions of specific iron compounds were pre-treated with 4 atm of H_2 for a designated time followed by addition of **1a**. Subsequent exposure to 1 atm of hydrogen and stirring at ambient temperature for 30 minutes (Scheme 10b). With 10 minutes of exposure of $^{(S)\text{-}tBu,Me}$ACNC)Fe(CH_2SiMe_3)$_2$, complete conversion of **1a** was observed in the subsequent catalytic hydrogenation and the resulting alkane was obtained in 75% *ee* (Scheme 10b, entry 1). Increasing the incubation time to 2 hours resulted in a lower enantiomeric excess of 60% (Scheme 10b, entry 2). With 48 hours of pretreatment, an additional, albeit slight drop in *ee* to 56% was observed (Scheme 10b, entry 4). By comparison, pretreatment of the neopentyl variant, ($^{(S)\text{-}tBu,Me}$ACNC)Fe(CH_2CMe_3)$_2$(N_2) for 2 hours produced lower conversion (76%) and enantiomeric excess (40%), suggesting that the decomposition products from background hydrogenolysis of $^{(S)\text{-}tBu,Me}$ACNC)Fe(CH_2SiMe_3)$_2$ and ($^{(S)\text{-}tBu,Me}$ACNC)Fe(CH_2CMe_3)$_2$(N_2) are different or are formed at different rates. These results account for the observed inverse dependence of H_2 pressure on enantioselectivity and also explain why more hindered, slower to react alkenes are reduced with lower selectivity; otherwise, decomposition of the active catalyst results in reduced enantioselectivity.

Scheme 10. A. Sequential hydrogenation-carbonylation of $^{(S)\text{-}tBu,Me}$ACNC)Fe(CH_2SiMe_3)$_2$ in the absence of alkene substrate. **B.** Hydrogenation of **1a** from H_2 pretreated iron com-

plexes.

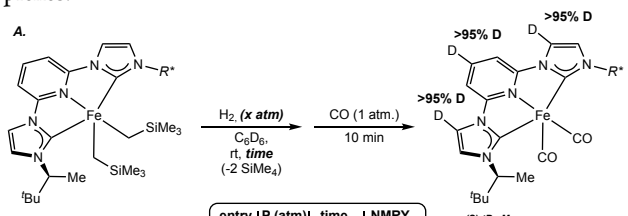

entry	P (atm)	time	NMRY
1	1	10 min	82%
2	4	10 min	42%
3	1	30 min	64%
4	1	2 h	55%
5	1	20 h	54%

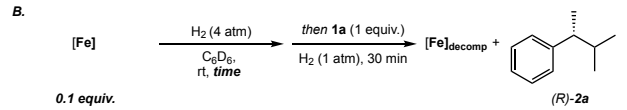

entry	[Fe]	time	% conv. 1a	% ee
1	$^{(S)\text{-}tBu,Me}$ACNC)Fe(CH_2SiMe_3)$_2$	10 min	>95	75
2	$^{(S)\text{-}tBu,Me}$ACNC)Fe(CH_2SiMe_3)$_2$	2 h	>95	60
3	$^{(S)\text{-}tBu,Me}$ACNC)Fe(CH_2CMe_3)$_2$(N_2)	2 h	76	40
4	$^{(S)\text{-}tBu,Me}$ACNC)Fe(CH_2SiMe_3)$_2$	48 h	95	56

Based on these results, the inverse dependence of enantioselectivity is attributed to controlling the rate of productive hydrogenation to catalyst decomposition to the ill-defined unselective catalyst of unknown homogeneity ($[Fe]_{decomp}$). An explanation of this effect is presented in Scheme 11. At lower pressures of hydrogen, this decomposition rate is slowed resulting in a lower concentration of $[Fe]_{decomp}$ compared to the desired enantioenriched catalyst ($[Fe]_{enantio}$) and increased enantioselectivity is observed. This rationalization is also consistent with lower levels of enantioselectivity on any highly hindered, or trisubstituted alkene. Unselective hydrogenation with the decomposed catalyst is competitive with the enantioselective catalyst, and thus the enantioselectivity is eroded at higher pressures of H_2.

Scheme 11. Rationalization of inverse H_2 pressure dependence on enantioselectivity.

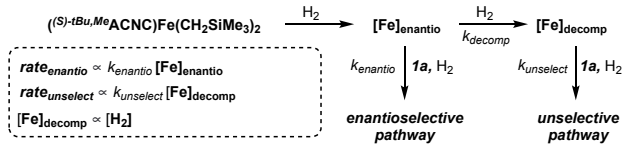

CONCLUSION

In conclusion, enantioenriched (ACNC)Fe dialkyl complexes have been prepared, structurally characterized and evaluated for their activity in the catalytic asymmetric hydrogenation of alkenes. The five-coordinate, S = 1 iron dialkyl complexes undergo reversible coordination of N_2 to form the corresponding S = 0, idealized octahedral derivatives. Enantioselectivity as high 70% *ee* was observed for the hydrogenation of **1a** and lower pressures of H_2 resulted in increased selectivity. In situ reaction monitoring and deuterium labeling studies established that alkene isomerization was not occurring on a timescale competitive with hydrogenation and was thereby eliminated as the origin of the observed pressure effect. Addition of the enamide methyl-2-acetamidoacrylate to a enantioenriched (ACNC)Fe dialkyl complex resulted in a crystallographically characterized product resistant to further reaction with H_2. Additional studies demonstrated that there is a dynamic, yet homogeneous speciation, however decomposition of the catalyst to a less selective form may be the source of the modest levels of enantioselectivity that were observed. These studies demonstrate that maintaining well-defined catalyst speciation is critical for enantioselective iron catalysis, a tridentate pincers, while successful still suffer from deleterious decomposition pathways. Importantly, maintaining well defined speciation guides the development of next-generation iron catalysts for asymmetric transformations.

ASSOCIATED CONTENT

Supporting Information

Complete experimental and computational details including precatalyst optimization studies, optimized structures, and characterization data for deuterated products. This material is available free of charge via the Internet at http://pubs.acs.org.

AUTHOR INFORMATION

Corresponding Author

* pchirik@princeton.edu

ORCID

Peter Viereck: 0000-0003-4691-8434
Stephan M. Rummelt: 0000-0003-3996-0271
Natalia A. Soja: 0000-0002-9635-748X
Tyler P. Pabst: 0000-0003-4595-2833
Paul J. Chirik: 0000-0001-8473-2898

Accession Codes

CCDC 2048706, 2048707, and 2048708

contain the supplementary crystallographic data for this paper. These data can be obtained free of charge via www.ccdc.cam.uc.uk/data_request/cif or by emailing data_request@ccdc.cam.ac.uk or by contacting the The Cambridge Crystallographic Data Center, 12 Union Road, Cambridge CB2 1EZ UK fax: + 44 1223 336033.

ACKNOWLEDGMENT

Financial support from a National Science Foundation (NSF) Grant Opportunities of Academic Liaison with Industry (GOALI) grant (CHE-1855719) is acknowledged.

REFERENCES

[1] (a) Shultz, C. S.; Krska, S. W. Unlocking the Potential of Asymmetric Hydrogenation at Merck. *Acc. Chem. Res.* **2007**, *40*, 1320–1326. (b) Saudan, L. A. Hydrogenation Processes in the Synthesis of Perfumery Ingredients. *Acc. Chem. Res.* **2007**, *40*, 1309–1319. (c) Ohkuma, T.; Kitamura, M.; Noyori, R. Asymmetric Hydrogenation. In *Catalytic Asymmetric Synthesis*; John Wiley & Sons, Ltd, **2005**; pp 1–110. (d) Asymmetric Catalysis on Industrial Scale: Challenges, Approaches and Solutions, 2nd ed.; Blaser, H.-U., Federsel, H.-J., Eds.; Mörlenbach: Wiley-VCH, 2010. (e) Knowles, W. S. Asymmetric hydrogenations (Nobel lecture). *Angew. Chem. Int. Ed.* **2002**, *41*, 1998–2007.

[2] (a) Cui, X.; Burgess, K. Catalytic Homogeneous Asymmetric Hydrogenations of Largely Unfunctionalized Alkenes. *Chem. Rev.* **2005**, *105*, 3272–3296. (b) Roseblade, S. J.; Pfaltz, A. Iridium-Catalyzed Asymmetric Hydrogenation of Olefins. *Acc. Chem. Res.* **2007**, *40*, 1402–1411. (c) Etayo, P.; Vidal-Ferran, A. Rhodium-Catalysed Asymmetric Hydrogenation as a Valuable Synthetic Tool for the Preparation of Chiral Drugs. *Chem. Soc. Rev.* **2012**, *42*, 728–754. (d) Verendel, J. J.; Pàmies, O.; Diéguez, M.; Andersson, P. G. Asymmetric Hydrogenation of Olefins Using Chiral Crabtree-Type Catalysts: Scope and Limitations. *Chem. Rev.* **2014**, *114*, 2130–2169. (e) Margarita, C.; Andersson, P. G. Evolution and Prospects of the Asymmetric Hydrogenation of Unfunctionalized Olefins. *J. Am. Chem. Soc.* **2017**, *139*, 1346–1356. (f) Shevlin, M. Practical High-Throughput Experimentation for Chemists. *ACS Med. Chem. Lett.* **2017**, *8*, 601–607.

[3] (a) Chirik, P. J. Iron- and Cobalt-Catalyzed Alkene Hydrogenation: Catalysis with Both Redox-Active and Strong Field Ligands. *Acc. Chem. Res.* **2015**, 48, 1687–1695. (b) Enthaler, S.; Junge, K.; Beller, M. Sustainable Metal Catalysis with Iron: From Rust to a Rising Star? *Angew. Chem.Int. Ed.* **2008**, *47*, 3317–3321. (c) Chen, J.; Lu, Z. Asymmetric Hydrofunctionalization of Minimally Functionalized Alkenes via Earth Abundant Transition Metal Catalysis. *Org. Chem. Front.* **2018**, *5*, 260–272. (d) Seo, C. S. G.; Morris, R. H. Catalytic Homogeneous Asymmetric Hydrogenation: Successes and Opportunities. *Organometallics* **2019**, *38*, 47–65.

[4] (a) Pony Yu, R.; Hesk, D.; Rivera, N.; Pelczer, I.; Chirik, P. J. Iron-Catalysed Tritiation of Pharmaceuticals. *Nature* **2016**, *529*, 195–199. (b) Obligacion, J. V.; Bezdek, M. J.; Chirik, P. J. C(sp^2)–H Borylation of Fluorinated Arenes Using an Air-Stable Cobalt Precatalyst: Electronically Enhanced Site Selectivity Enables Synthetic Opportunities. *J. Am. Chem. Soc.* **2017**, *139*, 2825–2832. (c) Pabst, T. P.; Obligacion, J. V.; Rochette, É.; Pappas, I.; Chirik, P. J. Cobalt-Catalyzed Borylation of Fluorinated Arenes: Thermodynamic Control of C(sp^2)-H Oxidative Addition Results in Ortho-to-Fluorine Selectivity. *J. Am. Chem. Soc.* **2019**, *141*, 15378–15389. (d) Corpas, J.; Viereck, P.; Chirik, P. J. C(Sp2)–H Activation with Pyridine Dicarbene Iron Dialkyl Complexes: Hydrogen Isotope Exchange of Arenes Using Benzene-d_6 as a Deuterium Source. *ACS Catal.* **2020**, *10*, 8640–8647. (e) Pabst, T. P.; Quach, L.; MacMillan, K. T.; Chirik, P. J. Mechanistic Origins of Regioselectivity in Cobalt-Catalyzed C(sp^2)-H Borylation of Benzoate Esters and Arylboronate Esters. *Chem* **2021**, *7*, 237–254.

[5] (a) Friedfeld, M. R.; Shevlin, M.; Hoyt, J. M.; Krska, S. W.; Tudge, M. T.; Chirik, P. J. Cobalt Precursors for High-Throughput Discovery of Base Metal Asymmetric Alkene Hydrogenation Catalysts. *Science* **2013**, *342*, 1076–1080. (b) Shevlin, M.; Friedfeld, M. R.; Sheng, H.; Pierson, N. A.; Hoyt, J. M.; Campeau, L.-C.; Chirik, P. J. Nickel-Catalyzed Asymmetric Alkene Hydrogenation of α,β-Unsaturated Esters: High-Throughput Experimentation-Enabled Reaction Discovery, Optimization, and Mechanistic Elucidation. *J. Am. Chem. Soc.* **2016**, *138*, 3562–3569. (c) Friedfeld, M. R.; Zhong, H.; Ruck, R. T.; Shevlin, M.; Chirik, P. J. Cobalt-Catalyzed Asymmetric Hydrogenation of Enamides Enabled by Single-Electron Reduction. *Science* **2018**, *360*, 888–893. (d) Zhong, H.; Friedfeld, M. R.; Chirik, P. J. Syntheses and Catalytic Hydrogenation Performance of Cationic Bis(Phosphine) Cobalt(I) Diene and Arene Compounds. *Angew. Chem. Int. Ed.* **2019**, *58*, 9194–9198. (e) Zhong, H.; Shevlin, M.; Chirik, P. J. Cobalt-Catalyzed Asymmetric Hydrogenation of α,β-Unsaturated Carboxylic Acids by Homolytic H2 Cleavage. *J. Am. Chem. Soc.* **2020**, *142*, 5272–5281. (f) Zhong, H.; Beromi, M. M.; Chirik, P. J. Ligand Substitution and Electronic Structure Studies of Bis(Phosphine)Cobalt Cyclooctadiene Precatalysts for Alkene Hydrogenation. *Can. J. Chem.* **2020** DOI: 10.1139/cjc-2020-0352.

[6] (a) Morello, G. R.; Zhong, H.; Chirik, P. J.; Hopmann, K. H. Cobalt-Catalysed Alkene Hydrogenation: A Metallacycle Can Explain the Hydroxyl Activating Effect and the Diastereoselectivity. *Chem. Sci.* **2018**, *9*, 4977–4982. (b) Hopmann, K. H. Cobalt–Bis(Imino)Pyridine-Catalyzed Asymmetric Hydrogenation: Electronic Structure, Mechanism, and Stereoselectivity. *Organometallics* **2013**, *32*, 6388–6399. (c) Renyuan Pony Yu, Jonathan M. Darmon, Carsten Milsmann, Grant W. Margulieux, S. Chantal E. Stieber, Serena DeBeer, and Paul J. Chirik . Catalytic Hydrogenation Activity and Electronic Structure Determination of Bis(arylimidazol-2-ylidene)pyridine Cobalt Alkyl and Hydride Complexes. *J. Am. Chem. Soc.* **2013,** *135*, 13168-13184.

[7] Broene, R. D.; Buchwald, S. L. Asymmetric Hydrogenation of Unfunctionalized Trisubstituted Olefins with a Chiral Titanocene Catalyst. *J. Am. Chem. Soc.* **1993**, *115*, 12569–12570.

[8] Troutman, M. V.; Appella, D. H.; Buchwald, S. L. Asymmetric hydrogenation of unfunctionalized tetrasubstituted olefins with a cationic zirconocene catalyst. *J. Am. Chem. Soc.* **1999**, *121*, 4916–4917

[9] Bianchini, C.; Mantovani, G.; Meli, A.; Migliacci, F.; Zanobini, F.; Laschi, F.; Sommazzi, A. Oligomerisation of Ethylene to Linear α-Olefins by New Cs- and C1-Symmetric [2,6-Bis(Imino)Pyridyl]Iron and -Cobalt Dichloride Complexes. *Eur. J. Inorg. Chem.* **2003**, *2003*, 1620–1631.

[10] (a) Monfette, S.; Turner, Z. R.; Semproni, S. P.; Chirik, P. J. Enantiopure C1-Symmetric Bis(Imino)Pyridine Cobalt Complexes for Asymmetric Alkene Hydrogenation. *J. Am. Chem. Soc.* **2012**, *134*, 4561–4564. (b) Friedfeld, M. R.; Shevlin, M.; Margulieux, G. W.; Campeau, L.-C.; Chirik, P. J. Cobalt-Catalyzed Enantioselective Hydrogenation of Minimally Functionalized Alkenes: Isotopic Labeling Provides Insight into the Origin of Stereoselectivity and Alkene Insertion Preferences. *J. Am. Chem. Soc.* **2016**, *138,* 3314–3324. (c) Viereck, P.; Krautwald, S.; Pabst, T. P.; Chirik, P. J. A Boron Activating Effect Enables Cobalt-Catalyzed Asymmetric Hydrogenation of Sterically Hindered Alkenes. *J. Am. Chem. Soc.* **2020**, *142*, 3923–3930.

[11] (a) Chen, J.; Chen, C.; Ji, C.; Lu, Z. Cobalt-Catalyzed Asymmetric Hydrogenation of 1,1-Diarylethenes. *Org. Lett.* **2016**, *18*, 1594–1597. (b) Zuo, Z.; Xu, S.; Zhang, L.; Gan, L.; Fang, H.; Liu, G.; Huang, Z. Cobalt-Catalyzed Asymmetric Hydrogenation of Vinylsilanes with a Phosphine–Pyridine–Oxazoline Ligand: Synthesis of Optically Active Organosilanes and Silacycles. *Organometallics* **2019**, *38*, 3906–3911. (c) Guo, J.; Shen, X.; Lu, Z. Regio- and Enantioselective Cobalt-Catalyzed Sequential Hydrosilylation/Hydrogenation of Terminal Alkynes. *Angew. Chem. Int. Ed.* **2017**, *56*, 615–618. (d) Chen, J.; Lu, Z. Asymmetric Hydrofunctionalization of Minimally Functionalized Alkenes via Earth Abundant Transition Metal Catalysis. Org. Chem. Front. 2018, 5, 260–272. (e) Cheng, Z.; Guo, J.; Lu, Z.

Recent Advances in Metal-Catalysed Asymmetric Sequential Double Hydrofunctionalization of Alkynes. *Chem. Commun.* **2020**, *56*, 2229–2239. (f) Chen, J.; Shen, X.; Lu, Z. Cobalt-Catalyzed Markovnikov Selective Sequential Hydrogenation/Hydrohydrazidation of Aliphatic Terminal Alkynes. *J. Am. Chem. Soc.* **2020**, *142*, 14455–14460.

[12] Hoyt, J. M.; Shevlin, M.; Margulieux, G. W.; Krska, S. W.; Tudge, M. T.; Chirik, P. J. Synthesis and Hydrogenation Activity of Iron Dialkyl Complexes with Chiral Bidentate Phosphines. *Organometallics* **2014**, *33*, 5781–5790.

[13] (a) Gopalaiah, K. Chiral Iron Catalysts for Asymmetric Synthesis. *Chem. Rev.* **2013**, *113*, 3248–3296. (b) Chen, J.; Xi, T.; Lu, Z. Iminopyridine Oxazoline Iron Catalyst for Asymmetric Hydroboration of 1,1-Disubtituted Aryl Alkenes. *Org. Lett.* **2014**, *16*, 6452–6455. (c) Chen, J.; Cheng, B.; Cao, M.; Lu, Z. Iron-Catalyzed Asymmetric Hydrosilylation of 1,1-Disubstituted Alkenes. *Angew. Chem. Int. Ed.* **2015**, *54*, 4661–4664. (d) Chen, J.; Lu, Z. Asymmetric Hydrofunctionalization of Minimally Functionalized Alkenes via Earth Abundant Transition Metal Catalysis. *Org. Chem. Front.* **2018**, *5*, 260–272. (e) Cheng, B.; Liu, W.; Lu, Z. Iron-Catalyzed Highly Enantioselective Hydrosilylation of Unactivated Terminal Alkenes. *J. Am. Chem. Soc.* **2018**, *140*, 5014–5017. (f) Chen, J.; Lu, Z. Asymmetric Hydrofunctionalization of Minimally Functionalized Alkenes via Earth Abundant Transition Metal Catalysis. *Org. Chem. Front.* **2018**, *5*, 260–272. (g) Pellissier, H. Recent Developments in Enantioselective Iron-Catalyzed Transformations. *Coord. Chem. Rev.* **2019**, *386*, 1–31. (h) Wen, H.; Liu, G.; Huang, Z. Recent Advances in Tridentate Iron and Cobalt Complexes for Alkene and Alkyne Hydrofunctionalizations. *Coord. Chem. Rev.* **2019,** 386, 138–153. (i) Chen, C.; Wang, H.; Sun, Y.; Cui, J.; Xie, J.; Shi, Y.; Yu, S.; Hong, X.; Lu, Z. Iron-Catalyzed Asymmetric Hydrosilylation of Vinylcyclopropanes via Stereospecific C-C Bond Cleavage. *iScience* **2020**, *23*, 100985. (j) Casnati, A.; Lanzi, M.; Cera, G. Recent Advances in Asymmetric Iron Catalysis. *Molecules*. **2020**, *25*, 3889. (k) Liang, Q.; Song, D. Iron N-heterocyclic carbene complexes in homogeneous catalysis. *Chem. Soc. Rev.* **2020**, *49*, 1209-1232.

[14] (a) Morris, R. H. Asymmetric Hydrogenation, Transfer Hydrogenation and Hydrosilylation of Ketones Catalyzed by Iron Complexes. *Chem. Soc. Rev.* **2009**, *38*, 2282–2291. (b) Tondreau, A. M.; Darmon, J. M.; Wile, B. M.; Floyd, S. K.; Lobkovsky, E.; Chirik, P. J. Enantiopure Pyridine Bis(Oxazoline) "Pybox" and Bis(Oxazoline) "Box" Iron Dialkyl Complexes: Comparison to Bis(Imino)Pyridine Compounds and Application to Catalytic Hydrosilylation of Ketones. *Organometallics* **2009**, *28*, 3928–3940. (c) Zuo, W.; Lough, A. J.; Li, Y. F.; Morris, R. H. Amine(Imine)Diphosphine Iron Catalysts for Asymmetric Transfer Hydrogenation of Ketones and Imines. *Science* **2013**, *342*, 1080–1083. (d) Li, Y.; Yu, S.; Wu, X.; Xiao, J.; Shen, W.; Dong, Z.; Gao, J. Iron Catalyzed Asymmetric Hydrogenation of Ketones. *J. Am. Chem. Soc.* **2014**, *136*, 4031–4039. (e) Bleith, T.; Wadepohl, H.; Gade, L. H. Iron Achieves Noble Metal Reactivity and Selectivity: Highly Reactive and Enantioselective Iron Complexes as Catalysts in the Hydrosilylation of Ketones. *J. Am. Chem. Soc.* **2015**, *137*, 2456–2459. (f) Li, Y.-Y.; Yu, S.-L.; Shen, W.-Y.; Gao, J.-X. Iron-, Cobalt-, and Nickel-Catalyzed Asymmetric Transfer Hydrogenation and Asymmetric Hydrogenation of Ketones. *Acc. Chem. Res.* **2015**, *48*, 2587–2598. (g) Wei, D.; Darcel, C. Iron Catalysis in Reduction and Hydrometalation Reactions. *Chem. Rev.* **2019**, *119*, 2550–2610. (h) Huber, R.; Passera, A.; Mezzetti, A. Which Future for Stereogenic Phosphorus? Lessons from P* Pincer Complexes of Iron(II). *Chem. Commun.* **2019**, *55*, 9251–9266. (h) Seo, C. S. G.; Morris, R. H. Catalytic Homogeneous Asymmetric Hydrogenation: Successes and Opportunities. *Organometallics* **2019,** *38*, 47–65

[15] (a) Bart, S. C.; Lobkovsky, E.; Chirik, P. J. Preparation and Molecular and Electronic Structures of Iron(0) Dinitrogen and Silane Complexes and Their Application to Catalytic Hydrogenation and Hydrosilation. *J. Am. Chem. Soc.* **2004**, *126*, 13794–13807. (b) Archer, A. M.; Bouwkamp, M. W.; Cortez, M.-P.; Lobkovsky, E.; Chirik, P. J. Arene Coordination in Bis(Imino)Pyridine Iron Complexes: Identification of Catalyst Deactivation Pathways in Iron-Catalyzed Hydrogenation and Hydrosilation. *Organometallics*. **2006**, *25*, 4269–4278. (c) Trovitch, R. J. Chirik, P. J. "Functional group tolerance and substrate scope in bis(imino)pyridine iron catalyzed alkene hydrogenation" *Organometallics.* **2008**, *27*, 1470-1478.

[16] (a) Danopoulos, A. A.; Wright, J. A.; Motherwell, W. B. Molecular N2 Complexes of Iron Stabilised by N-Heterocyclic 'Pincer' Dicarbene Ligands. *Chem. Commun.* **2005**, No. 6, 784–786. (b) Danopoulos, A. A.; Pugh, D.; Smith, H.; Saßmannshausen, J. Structural and Reactivity Studies of "Pincer" Pyridine Dicarbene Complexes of Fe0: Experimental and Computational Comparison of the Phosphine and NHC Donors. *Chem. Eur. J.,* **2009**, *15*, 5491–5502. (c) Pugh, D.; Wells, N. J.; Evans, D. J.; Danopoulos, A. A. Reactions of 'Pincer' Pyridine Dicarbene Complexes of Fe(0) with Silanes. *Dalton Trans.* **2009**, 7189–7195.

[17] (a) Yu, R. P.; Darmon, J. M.; Hoyt, J. M.; Margulieux, G. W.; Turner, Z. R.; Chirik, P. J. High-Activity Iron Catalysts for the Hydrogenation of Hindered, Unfunctionalized Alkenes. *ACS Catal.* **2012**, *2*, 1760–1764. (b) Yu, R. P.; Darmon, J. M.; Semproni, S. P.; Turner, Z. R.; Chirik, P. J. Synthesis of Iron Hydride Complexes Relevant to Hydrogen Isotope Exchange in Pharmaceuticals. *Organometallics* **2017**, *36*, 4341–4343. (c) Rummelt, S. M.; Darmon, J. M.; Yu, R. P.; Viereck, P.; Pabst, T. P.; Turner, Z. R.; Margulieux, G. W.; Gu, S.; Chirik, P. J. Synthesis, Structure, and Hydrogenolysis of Pyridine Dicarbene Iron Dialkyl Complexes. *Organometallics* **2019**, *38*, 3159–3168.

[18] The "A" designator before the CNC abbreviation signifies an alkyl rather than aryl *N*-imidazole substituent.

[19] Cámpora, J.; Naz, A. M.; Palma, P.; Álvarez, E.; Reyes, M. L. 2,6-Diiminopyridine Iron(II) Dialkyl Complexes. Interaction with Aluminum Alkyls and Ethylene Polymerization Catalysis. *Organometallics* **2005**, *24*, 4878–4881.

[20] Fernández, I.; Trovitch, R. J.; Lobkovsky, E.; Chirik, P. J. Synthesis of Bis(Imino)Pyridine Iron Di- and Monoalkyl Complexes: Stability Differences between $FeCH_2SiMe_3$ and $FeCH_2CMe_3$ Derivatives. *Organometallics* **2008**, *27*, 109–118.

[21] Sun, Y.; Landau, R. N.; Wang, J.; LeBlond, C.; Blackmond, D. G. A Re-Examination of Pressure Effects on Enantioselectivity in Asymmetric Catalytic Hydrogenation. *J. Am. Chem. Soc.* **1996**, *118*, 1348–1353.

For Table of Contents Use

Enantioenriched Iron Complexes For Asymmetric Alkene Hydrogenation

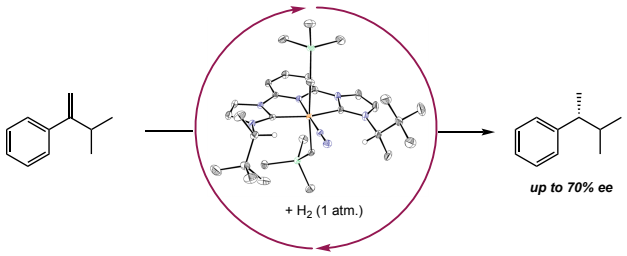

Stoichiometric Reactivity - Catalytic Activity - Catalyst Decomposition Studies